Food Hydrocolloids 154 (2024) 110149

Contents lists available at ScienceDirect

Food Hydrocolloids

journal homepage: www.elsevier.com/locate/foodhyd

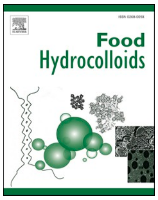

Effects of cellulose diameter on the formation and rheological properties of edible walnut oleogels structured by cellulose nanofiber

Yuxuan Zou [a,c,d,1], Yang Tian [a,c,d,e,1], Bing Zhao [a,c,d], Jienan Li [f], Jia Luo [b,*], Jun Sheng [c], Xiufen Li [a,c,d,**]

[a] College of Food Science and Technology, Yunnan Agricultural University, 425 Fengyuan Road, Kunming, 650201, Yunnan, People's Republic of China
[b] Kunming Branch, CAS Key Laboratory of Tropical Plant Resource and Sustainable Use, Xishuangbanna Tropical Botanical Garden, Chinese Academy of Sciences, 88 Xuefu Road, Kunming, 650223, Yunnan, People's Republic of China
[c] Engineering Research Center of Development and Utilization of Food and Drug Homologous Resources, Ministry of Education, Yunnan Agricultural University, 425 Fengyuan Road, Kunming, 650201, Yunnan, People's Republic of China
[d] Yunnan Key Laboratory of Precision Nutrition and Personalized Food Manufacturing, Yunnan Agricultural University, 425 Fengyuan Road, Kunming, 650201, Yunnan, People's Republic of China
[e] Pu'er University, Pu'er 665000, China
[f] Yunnan Institute of Medical Device Testing, 616 Kefa Road, Kunming, 650101, Yunnan, People's Republic of China

ARTICLE INFO

Keywords:
Cellulose nanofiber
Particle diameter
Walnut oil
Oleogels
Rheology

ABSTRACT

Oleogel of edible vegetable oils structured by cellulose nanofiber (CNF) via emulsion-templated method has attracted many interests due to its potential substitute of saturated or *trans*-fats in food industry. The gelation mechanism of liquid oil is dominated by different intermolecular non-covalent interactions, while the type and strength of these interactions are greatly influenced by the structure and properties of the gelator factors. Here, the effect of different CNF diameter ranges (5–10 nm, 10–20 nm and 20–60 nm) was investigated for CNF-based walnut oil oleogels, under the same fiber length and surface carboxyl content of CNFs. The results showed that CNFs with diameters of <20 nm exhibited better emulsification properties, and effectively restrained droplet size increasing and aggregation, compared to CNF with diameter of 20–60 nm. The resultant oleogels with smaller CNF diameter exhibited higher oil-binding capacity (OBC, ~85%) and better thermal stability of the resultant oleogels. More compact structure and stronger mechanical strength of oleogels were achieved with CNF diameters of <20 nm, which was verified by stronger textural hardness of the oleogels (0.46 N), as well as higher storage modulus (up to 1.1×10^5 Pa) and apparent viscosity in rheological measurement. The enhanced OBC and structure strength of oleogels with smaller CNF diameter could be attributed to the enhanced hydrogen bonding interactions between CNF molecules and CNFs with oil molecules during oleogelation, as the rigorously fibrillation exposed more surface hydroxyl groups as accessible hydrogen bonding sites during CNF preparation. This study improved the understanding about gelling properties of CNFs with different fiber diameters and provided an empirical basis for the construction of CNF-based oleogels with tunable hydrogen bonding interactions.

1. Introduction

Oleogel is a semisolid or solid-like gel formed by incorporating edible liquid oil into a well-organized three-dimensional network under the assistance of structurant or oleogelator. Oleogel can be used as novel healthier fat substitute for partially or totally replacing saturated or *trans*-fats in food products, such as cheese, cookies, chocolate, ice cream, sausage, etc. (Hu, Jiang, Du, & Meng, 2023; Zhao, Wei, & Xue, 2021). The oleogelator is crucial to promoting the formation of oleogel from liquid oil (Wang et al., 2023). Due to safe and plentiful raw material, oleogels fabricated by polysaccharide as oleogelator have become novel strategy to replace solid fats and meet the need of embedding and

---

* Corresponding author.
** Corresponding author. College of Food Science and Technology, Yunnan Agricultural University, 425 Fengyuan Road, Kunming, 650201, Yunnan, People's Republic of China.

E-mail addresses: luojia@xtbg.ac.cn (J. Luo), orangexiufen@163.com (X. Li).

[1] These authors contributed equally to this paper.

https://doi.org/10.1016/j.foodhyd.2024.110149
Received 8 March 2024; Received in revised form 22 April 2024; Accepted 26 April 2024

delivering varied nutrition or flavors (Li et al., 2023, 2024). Recently, cellulose and its derivatives with oleophilic properties, such as methylcellulose (MC) and ethylcellulose (EC), or with enhanced hydrophilicity, like microcrystalline cellulose, carboxymethyl cellulose (CMC), hydroxylpropyl methyl cellulose (HPMC), regenerated cellulose (RC) and several natural fibers have also been reported to produce oleogels with controllable viscoelasticity (Li et al., 2023, 2024).

Among them, cellulose nanofiber (CNF) has attracted rapidly growing scientific and technological interest from both academic and industrial researchers, due to its biodegradability, biocompatibility and thermal stability (Du et al., 2019). It achieves considerable applications in food industry as food additive, emulsifier, nutraceuticals carrier of bioactive compounds or as natural coating or packaging films (Habibi, Lucia, & Rojas, 2010; Ni, Fan, & Sun, 2020). As renewable polymer with diameter of less than 100 nm prepared from natural cellulose, CNF are of great interest among the anisotropic particles used for stabilizing emulsions (Yu, Peng, & Wu, 2024). In our previous study, walnut oleogels were successfully prepared by CNFs as the unique oleogelator using emulsion template approach. The CNF-based walnut oleogels exhibited high gel strength and thermal stability.

The types and properties of cellulose nanomaterials, including cellulose size (e.g. length), flexibility, surface acetylation and carboxyl degree of substitution, affect the emulsifying or gelling properties of cellulose nanomaterials. In Pickering emulsions, cellulosic nanofiber plays different roles during emulsification. Flexible bacterial cellulose (BC) has nearly no emulsifying capacity, whereas semi-flexible cellulose nanofiber (CNF) and rigid cellulose nanocrystal (CNC) can be well used to stabilize emulsions (Perumal, Nambiar, Moses, & Anandharamakrishnan, 2022). In sunflower seed oil-in-water Pickering emulsions, the emulsifying ability of acetylated chitin nanocrystals (ChNCs) were affected by the surface acetylation of chitin nanocrystals (Velásquez-Cock et al., 2019), in which the acetylation with moderate degree of substitution (0.38) reduced hydrophilicity and increased surface charge level of ChNCs, and therefore significantly improved the emulsifying ability of ChNCs. In corn oil-in-water emulsion, interfacial properties of cellulose nanofiber was affected by nanoparticle length, while a discontinuous monolayer was more likely formed with short nanofibers after adsorbing at the oil/water interface (Piao et al., 2022). In surimi gel, the reinforcement of carboxymethylated CNF in surimi gel structure was greatly depended on the surface charge, in which CNF with 0.72 mmol/g carboxyl substitution degree displayed the maximum hardness value and lowest water mobility (Lu, Li, Ge, Xie, & Wu, 2021). However, for oleogel, the effect of nanocellulose particle characteristic was not discussed before, although this effect might affect the practicality of the prepared CNF-based oleogel, in particular its oil-binding stability, texture, processing characteristics or other properties when it was used as fat substitute.

In this study, three CNFs with particle diameters of 5–10 nm, 10–20 nm and 20–60 nm were used to prepare walnut oil-in-water emulsions. Then the emulsions were used as template to prepare soft oleogels after following freeze-dehydration. The objective was to disclose the effect of fiber diameter on the structure and properties of the constructed oleogels. For structure characterization, XRD, FTIR and cryo-SEM were employed. For the determination of mechanical properties, textural and rheological analyses including strain sweep, frequency sweep, flow measurement, time sweep, and temperature sweep were comprehensively conducted. This work will advance the knowledge of tailoring nanocellulose on the plant oil oleogels by regulating fiber size.

2. Materials and methods

2.1. Materials

Cellulose nanofibers (CNFs, length of 0.8–2.0 μm, carboxyl group of 1.80 mmol/g, particle diameters of 5–10 nm, 10–20 nm and 20–60 nm, respectively) at 1.0% (w/w) aqueous solution was purchased from Woodelfbio biological technology co., Ltd (Tianjing, China). Hot pressed walnut oil was purchased from Dianxue Grain and Oil Co., Ltd. (Yunnan, China). High purity water with an electrical conductivity of 12–18.2 mΩ cm was supplied by a laboratory water purifier (FST-JY-80). All other chemicals used were analytical grade.

2.2. Preparation of CNF-based emulsions and oleogels

The preparation procedure of CNF-based oleogels with different CNF diameters could refer to our previously published work (Li et al., 2023). Briefly, CNF-based walnut oil emulsion was firstly prepared by high-speed homogenizer (HR-500, Huxi, China) and high-speed disperser (Ultraturrax, IKA, Germany), with the volume ratio of water to walnut oil of 4/1 and CNF concentration of 0.12–0.28%. Then, the emulsions were dried into soft solids in a vacuum freeze-dryer (FD-1) for more than 48 h. And the oleogels were obtained by shearing with a grinder (10, 000 rpm, 30 s).

2.3. Surface tension of CNF dispersion

The determination of surface tension was based on the dataphysics DCAT11 tensiometer (Hamburg, Germany). The Wilhelmy plate (19.9 mm × 10 mm × 0.2 mm) was used to determine the surface tensions at the air-sample surface of the CNF dispersion with different fiber diameters. Each sample was prepared by the same method for emulsion preparation as described in Section 2.2. The surface tension of deionized water (72.2 ± 0.3 mN m^{-1}) was measured before testing the emulsion samples. The test was conducted until the surface tension value of the measured samples reproduced to an accuracy of ±0.03 mN m^{-1}. The experiments were performed at five times at 25 °C.

2.4. Appearance and microstructure observation of emulsions

The freshly prepared emulsion was poured into a small plastic bottle (20 mL) and photographed with a digital camera after standing for 0.5 h and 24 h at room temperature. An inverted microscope (Olympus CX43RF, Tokyo, Japan) equipped with a digital camera (Nikon, Japan) was used to observe the shape and arrangement of emulsion droplets. Emulsion samples (20 μL) were spread on a microscopy slide and overlaid with a coverslip. All images were captured under 100 × 10 magnification.

2.5. Interfacial tension, ζ-potential and droplet size of emulsions

Zeta-potential and droplet size measurement. Droplet size of the CNF-based walnut oil emulsions was determined by Mastersizer 3000 (Malvern Instruments, Worcestershire, UK). A 100-fold dilution of emulsions with distilled water was performed before ζ-potential measurement by a multi-angle particle size and zeta potential analyzer (NanoBrook Omni, Brookhaven, USA). The refractive index of water was set as 1.33. The samples were equilibrated in the apparatus for 180 s prior to testing.

Interfacial tension measurement. The interfacial tension of the aqueous CNF-oil interface was measured using an optical drop shape tensiometer (OCA-20, DataPhysics, Germany). A glass container was half-filled with walnut oil. The density of the soybean oil was 0.894 g/mL. A pendant drop (~20 μL) of sample solution was formed by a syringe needle which was immersed in walnut oil. The shape of the pendant drop was recorded by a CCD camera and the interfacial tension value was calculated by SCA20 software (DataPhysics, Germany) according to the Young-Laplace equation. The pure water was used as a reference.

2.6. Oil binding capacity and oil loss determination

The details of OBC and OL measurements could be seen from the previous method (Li et al., 2024). A centrifugation method was followed to determine the oil binding capacity (OBC) of the final oleogel samples and the oil loss (OL) of oleogels after processing at different temperatures.

2.7. Fourier transform-infrared spectroscopy (FTIR) and X-ray diffraction (XRD)

The FTIR samples were prepared by mixing and grinding an appropriate amount of oleogel sample with dried KBr powder to make a press tablet. The walnut oil sample was uniformly coated on the surface of the KBr pressed tablets. Cellulose samples were freeze-dried to form powder and mixed with KBr powder to make press tablets for testing. The test conditions were as follows: scanning at 25 °C, wavenumber range of 400–4000 cm^{-1}, resolution of 4 cm^{-1}, and 32 scans to take the average value.

The crystal structures of CNF powders and oleogel samples were analyzed by X-ray diffractometer (Ultima IV, Rigaku, Japan) using a Cu-based X-ray radiation source. Measurements were made at room temperature. Diffractograms were obtained at diffraction angles (2θ) in the range of 5°–60° with a scanning rate of 4°/min, and data were collected and analyzed using MDI Jade 6 (Materials data Inc., Livermore, USA) software. The crystallite size (D, Å) and short spacing (d, Å) of the oleogel particles were calculated as the previous method (Li et al., 2023).

2.8. Microstructure observation of oleogels

Analysis was performed by cryo-scanning electron microscopy (Cryo-SEM). Samples were flash frozen by immersion in liquid nitrogen and transferred to a cryogenic unit (Quorum PP3000T, UK) connected to a scanning electron microscope (FEI Quanta 450, Japan). The specimens were sublimated and gold-plated, and then observed under a sample stage at −140 °C, 10 kV.

2.9. Rheological measurement

A rotational rheometer (MCR 302, Anton Paar, Graz, Austria) with stress controlled model was used to measure the rheological properties of the samples. A parallel plate with a diameter of 25 mm and a gap of 1 mm was used. Dynamic oscillatory tests, including strain sweep, frequency sweep, flow measurement, time sweep and temperature sweep, were used. Strain sweep were performed with strains ranging from 0.001% to 100% at the frequency of 1 Hz to determine the linear viscoelastic region (LVR) limit and yield stress. Then, frequency sweep (0.01–100 Hz) was performed at the constant strain of 0.02% within the LVR. Flow measurement was conducted to determine the flow properties of the oleogels at a fixed strain (0.02%) and a shear rate of 0.1–100 s^{-1}. The thixotropic behavior was further measured by a three-stage thixotropic test (3ITT) with alternative cycles of low and high shear rates (20 s at shear rate of 0.1 s^{-1} for the first stage, then 10 s^{-1} for 20 s, and finally 0.1 s^{-1} for 1 min). Temperature sweep (from 20 to 90 °C, rate of 5 °C/min, 1 Hz) was performed at a constant strain of 0.02%. The details of calculations could be seen from the previous method (Li et al., 2024). All measurements were performed at 25 °C. The reported data points were average values of at least three repeated measurement results, except twice repeats for time sweep.

2.10. Texture analysis

Sheared oleogel samples were used for texture measurements. The samples were placed in cylindrical containers (inner diameter 30 mm × height 15 mm) and equilibrated at room temperature for 1 day. Penetration tests were performed using an FTC/TMS-Touch texture analyzer (Food Technology Corporation, USA) and a 50 N load cell. The samples were penetrated with a cylindrical probe with a diameter of 10 mm at a trigger force of 0.05 N. The penetration depth was 6 mm and the velocity was 1 mm/s. Force-time profiles were recorded to calculate the maximum force and the area under the curve (AUC). The reported values were averaged over three repetitions.

2.11. Statistical analysis

Statistical analysis was performed using IBM SPSS software (SPSS; Inc., Armonk, NY, USA). All data available are presented as mean and standard deviations. One-way analysis of variance (ANOVA) of means (Duncan's test, $p < 0.05$) was used to evaluate significant differences among samples.

3. Results and discussion

3.1. Average particle size, ζ-potential, and storage stability of CNF-based emulsions with different CNF diameters

To fabricate CNF-based oleogels by emulsion-templated method, the emulsions with different CNF diameters were prepared first at CNF concentrations of 0.12–0.28%. Average particle size, ζ-potential, and storage stability of CNF-based emulsions were analyzed. The smaller the droplet size, the higher the stability against droplet aggregation and flocculation (Dickinson, 2019). In Fig. 1A, the freshly prepared emulsions were milky white and well dispersed at the studied CNF loadings. No phase separation was observed at least within half an hour. This benefited from the hydrophilicity of cellulose and the corresponding three-point contact angle of CNF at the O/W interface, which made the bending of the O/W interface facilitating the formation of positive curvature toward the organic phase, and resulted in the formation of water-continuous O/W emulsions (Carrillo, Nypelö, & Rojas, 2015). This result confirmed CNF as an effective stabilizer for the formation of O/W emulsions. After 24 h of storage, all the three CNF materials lose emulsifying ability to walnut oil/water system at CNF concentration of 0.12% (Table 1). CNF with diameters of 5–10 nm and 10–20 nm could emulsify walnut oil with CNF loading of higher than 0.16%. In contrast, CNF with diameter of 20–60 nm could only emulsify oil with much higher CNF concentrations of ≥0.24%. These results were consistent with the result of acetylated chitin nanocrystals (ChNCs) stabled emulsion in literature (Yu et al., 2024). The shorter ChNCs diameter (18.5 *vs.*22.5 nm) resulted in smaller droplet size of the emulsions (255 *vs.* 342 nm).

This difference was closely related to the changed size properties of CNF. Smaller CNF diameters showed good resistance to aggregation and move upwards to the surface. This could be attributed to the fact that CNF covered the surface of oil droplets, and protected droplets from aggregation by generating a strong spatial repulsion (Lv, Zhou, Bai, Rojas, & McClements, 2021). The decrease in droplet size and the formation of a thick protective coating greatly improved the stability of the emulsion (Lee, Wi, & Choi, 2023). Fig. 1B and C presented the changes in the morphology and droplet size of emulsions, and further verified the above inferences. A remarkably bimodal pattern was observed for the droplet size distribution of emulsions in Fig. 1C, which was attributed to the contributions from CNF and the minor surface-active components in walnut oil, respectively. For the main peak at about 8–300 μm that contributed by CNF, the emulsions stabilized with CNF diameters of 5–10 and 10–20 nm provided significantly smaller droplet size than those in the emulsion with CNF diameter of 20–60 nm. In Table 2, the particle sizes (D [4,3]) of emulsions with CNF diameters of 5–10 nm and 10–20 nm were 28.73 and 24.13 μm, respectively. However, a significantly ($p < 0.05$) increasing in D [4,3] value (36.08 μm) was for the emulsion with CNF diameter of 20–60 nm. It was also clearly seen that droplets aggregated in clusters in the emulsion with CNF diameter of 20–60 nm (Fig. 1B).

The use of ζ-potential was to examining the stability of a dispersed system. The ζ-potential thresholds between unstable and stable systems are considered as follows: the ζ-potential of very unstable, relatively stable, moderately stable and highly stable systems are in the range of

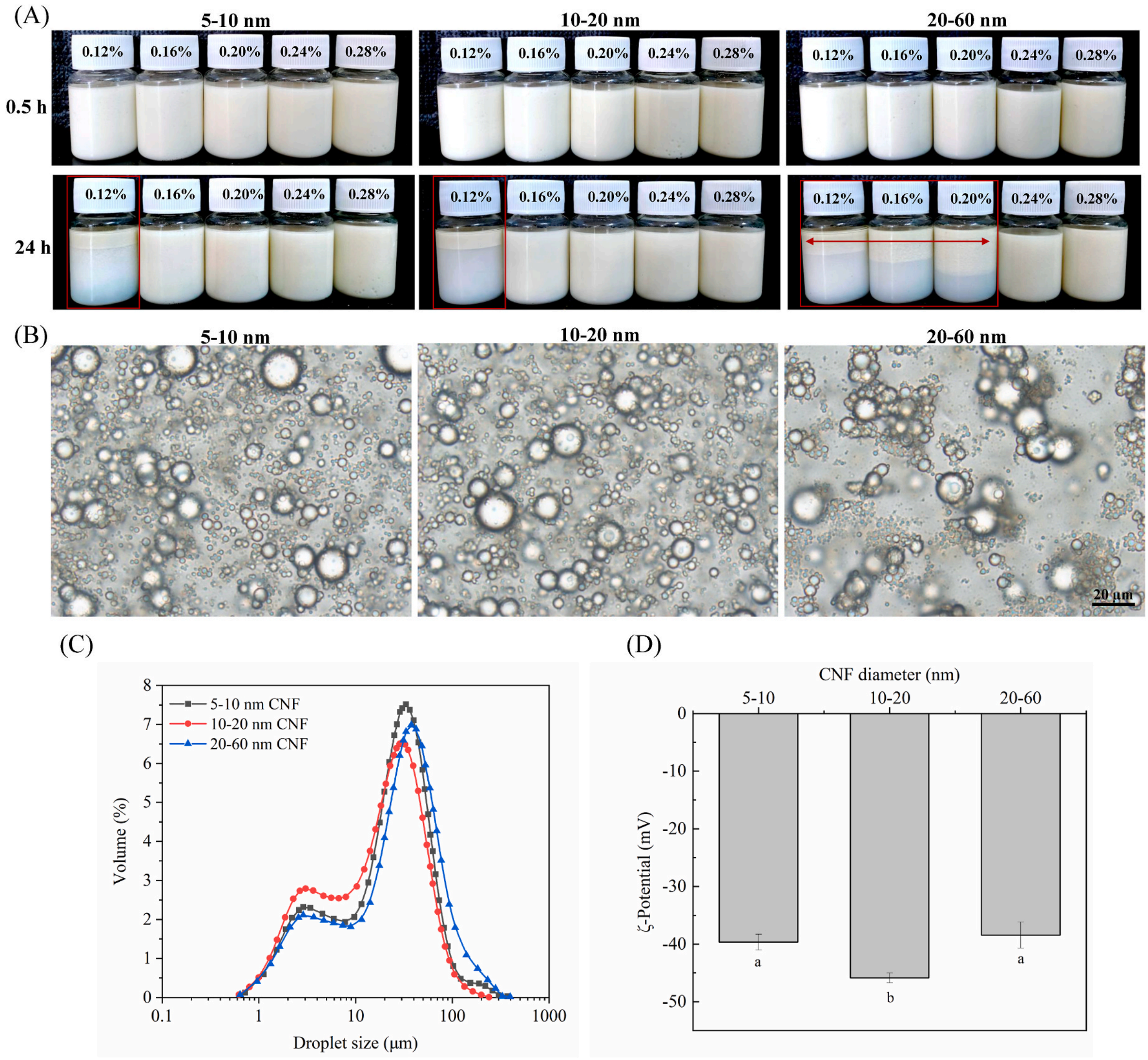

Fig. 1. Digital pictures (A), optical micrographs (B), droplet size distribution (C) and ζ-potential (D) of the walnut oil-in-water emulsions (volume ratio of water to walnut oil = 4:1) stabilized by CNFs with various diameters. Different letters (a–c) indicate significant differences ($p < 0.05$).

Table 1
Phase behavior of the walnut oil-in-water emulsions (volume ratio of water to walnut oil = 4:1) stabilized by CNFs with different CNF diameters after 24 h storage.

CNF diameter (nm)	CNF concentration				
	0.12%	0.16%	0.20%	0.24%	0.28%
5–10	×	✓	✓	✓	✓
10–20	×	✓	✓	✓	✓
20–60	×	×	×	✓	✓

Note: × indicates obvious phase separation, while √ means no evident creaming.

0–10, 10–20, 20–30 and 30 mV (Cano-Sarmiento et al., 2018). In Fig. 1D, All the absolute ζ-potential values of CNF-based emulsions were larger than 30 mV, indicating that the emulsion system had excellent stability (Cano-Sarmiento et al., 2018; Carrillo et al., 2015). Among the three emulsions, the ζ-potential value of the emulsion with CNF diameter of 10–20 nm achieved the maximum of −45.86 mV, which meant that the attractive and repulsive forces between particles were balanced, resulting in the stability of the dispersed system. The specific range of CNF diameter (10–20 nm) was in favor of the stabilization of the emulsion system. This was due to the appropriately positively charged CNF molecules with medium diameter could be electrostatic absorbed on the interface of walnut oil droplets, and formed a sufficient layer to cause electrostatic repulsion and steric hindrance effect, which resisted the aggregation and thus improved the stability of walnut emulsion. This was consistent with the phenomenon in the case of xanthan gum (Zhu et al., 2024).

Table 2
Droplet size of walnut oil-in-water emulsions (volume ratio of water to walnut oil = 4:1) stabilized by CNFs with different diameters.

CNF diameter (nm)	Dx (10) (μm)	Dx (50) (μm)	Dx (90) (μm)	D [4,3] (μm)	D [3,2] (μm)
5–10	2.71 ± 0.02 ^{b}	23.60 ± 0.20 ^{b}	59.18 ± 0.90 ^{b}	28.73 ± 0.79 ^{b}	7.99 ± 0.09 ^{b}
10–20	2.42 ± 0.01 ^{c}	18.58 ± 0.15 ^{c}	53.20 ± 0.41 ^{c}	24.13 ± 0.33 ^{c}	6.83 ± 0.03 ^{c}
20–60	2.79 ± 0.02 ^{a}	27.90 ± 0.37 ^{a}	77.63 ± 2.29 ^{a}	36.08 ± 1.09 ^{a}	8.45 ± 0.09 ^{a}

3.2. *Surface tension and interfacial tension of CNF-based emulsions with different diameters*

Surface tension and interfacial tension are closely related to the stability and applicability of emulsion systems. Surface tension is an important parameter to evaluating the emulsifying performance of surfactants in emulsions. Surface tension of the 0.4% CNF aqueous solution was tested by Wilhelmy plate method, with the results shown in Fig. 2A. The aqueous solution with CNF diameter of 5–10 nm showed the highest surface tension value (71.5 mN m^{-1}), which was close to the surface tension of pure water (72.2 mN m^{-1}).With the increase of CNF diameter size, the surface tension was decreased, which was attributed to the decrease of CNF hydrophilicity. The hydrophilicity of CNF molecules produced accessorial cohesive force to the water molecules at water-air interface, which forced the interface to be blended with higher curvature, while the molecules at the interface needed more tension or energy to minimize the interface area.

Simultaneously, interfacial tension of walnut oil-CNF aqueous solution (0.32%) system was determined by pendant drop method, which is conducive to understanding the interfacial properties of emulsion. The interfacial tension of walnut oil-CNF aqueous solution with different CNF diameters was shown in Fig. 2B. The increase in CNF diameter (20–60 nm) enhanced the interfacial tension of the emulsion system, compared to the emulsions with CNF diameters of 5–10 and 10–20 nm. It is generally believed that the tension at the O/W interface is controlled by the adsorption of surface-active substances (both CNF from the aqueous phase and trace components from the oil phase) at the interface, while it is determined by two factors: the type and chemical properties of the active substance and the amount of the active substance adsorbed at the interface. For instance, the amount of CNFs adsorbed on the oil droplet surface (AA) is a function of the O/W interfacial free energy (G) (Goi et al., 2019). For CNF factor, during the preparation of CNF by TEMPO process (2,2,6,6-tetramethylpiperidinyl-1-oxyl), with the increased rigorously fibrillation reaction, cellulose per unit mass generated fibers with finer diameters but higher numbers. As a result, more hydroxyl groups originally embedded inside the cellulose bundles are exposed, which increases the hydrophilicity of the CNF factor, and also provides more hydroxyl sites for stabilizing the O/W interface. Since the surface carboxyl content of CNFs used in this study was fixed (1.80 mmol/g), it meant that the same number of surface hydroxyl groups was converted to -COONa functionality during the TEMPO process, regardless of the CNF particle diameter was 5–10 or 20–60 nm. Therefore, the number of available surface hydroxyl groups per unit mass of CNF was remarkably less for the CNF with particle diameter of 20–60 nm. This resulted in a significantly higher O/W interfacial tension for the system with CNF diameter of 20–60 nm than that with CNF diameter of <20 nm. More seriously, in the system with CNF diameter of 20–60 nm, due to the lack in available hydroxyl groups of CNF, the dominant mechanism for stabilizing O/W interface was possibly the -COONa functionality on the CNF surface and the hydroxyl group originated from the minor polyphenol component in walnut oil (Cong, Zhang, Liu, & Huang, 2020). However, the chemical binding between these two functional groups might further weaken the ability of them to stabilizing the interface, which resulted in a slightly higher tension value of the system with CNF diameter of 20–60 nm than that of pure water-walnut oil system (27.7 vs 27.4 mN m^{-1}).

On the other hand, the further reduction of CNF diameter from 10-20 nm to 5–10 nm might increase the positively charge density on CNF surface, which reversely limited both their adsorption and surface coverage (Arcari, Geue, Mezzenga, Nyström, & Fischer, 2019). Or, the further reduction of CNF diameter to 5–10 nm made the CNF factor excessive hydrophilicity (Fig. 2B) or unfavorable contact angle at O/W interface (Arcari et al., 2019), which resulted in much less adsorption of CNF molecules at the interface of oil droplets.

In brief, the adsorption of charged anisotropic nanocellulose particles at O/W interfaces was regarded as the complex interplay of particle and interface charges, particle wetting, ionic strength in aqueous phase, as well as the properties of oil phase such as its polarity and interface tension (Bergfreund, Sun, Fischer, & Bertsch, 2019; Ni et al., 2020). CNF with diameter of 20–60 nm possibly provided bad interfacial charge structure for stabilizing the O/W interface, while unfavorable particle wetting affected the interfacial adsorption of CNF with diameter of 5–10 nm. As a result, among the three systems with different CNF diameters, the lowest interfacial tension (11.4 mN m^{-1}) was detected for the case with CNF diameter of 10–20 nm.

3.3. *Oleogel morphology*

Fig. 3 demonstrated the cryo-SEM image of the freeze-dried oleogel samples, in which oil droplets could be seen closely packed together in a non-spherical shape. It indicated that the microstructure of the dried product was still largely preserved in the sheared oleogel (Patel et al., 2014). The oleogels with CNF diameters of 5–10 nm and 10–20 nm were well structured, with the individual oil droplets separated by the gel network. In contrast, the oleogel images with CNF diameter of 20–60 nm showed irregular shapes and the boundaries between the oil droplets disappeared, suggesting that aggregation of the oil droplets occurred during drying, resulting in an inhomogeneous gel structure, which also occurred in the study of Bascuas et al. (Bascuas, Hernando, Moraga, & Quiles, 2019).

3.4. *Oil-binding capacity and oil loss of oleogels*

Oil-binding capacity (OBC), an important feature for evaluating the macroscopic properties of oleogels, reflects the ability of a structured network to cramping liquid oil. The effect of CNF diameter on the OBC

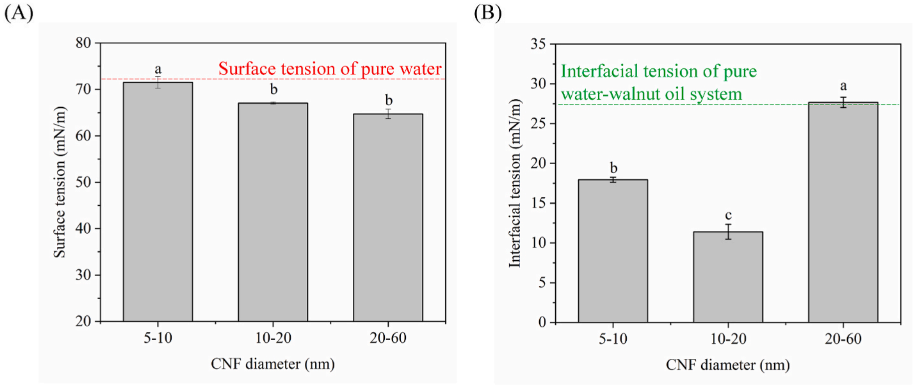

Fig. 2. Surface tension of 0.4% CNF aqueous solution by Wilhelmy plate method (A). Interfacial tension of walnut oil-CNF aqueous solution (0.32%) system by pendant drop method (B).

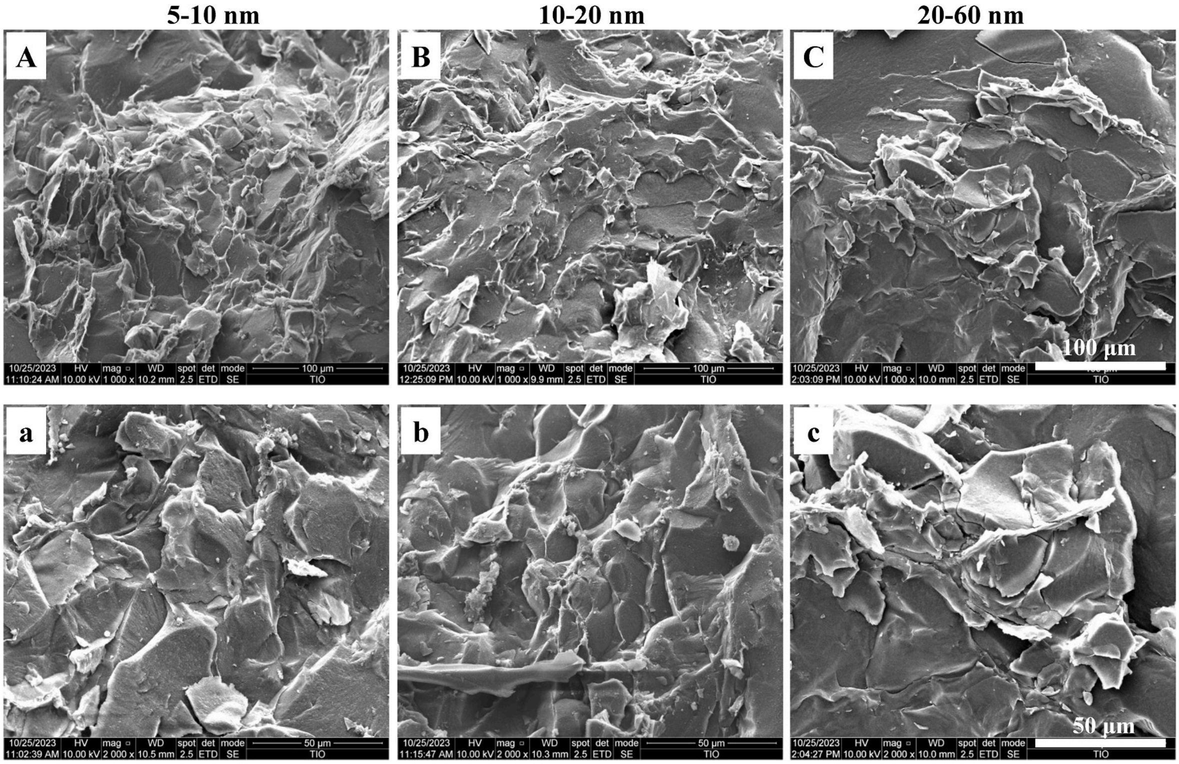

Fig. 3. Scanning electron microscopic images of oleogels with various CNF diameters. Images were taken at 1000 × and 2000 × .

values of oleogels was shown in Fig. 4, and the values of all oleogels were above 75%. This was the result of the dense and stable three-dimensional network structure of the oleogels, as reflected by cryo-SEM images (Fig. 3). CNFs with diameters of 5–10 nm and 10–20 nm constructed oleogels in OBC values with less significant difference (85.5% and 85.1%, respectively). However, the OBC value of oleogel with CNF diameter of 20–60 nm decreased dramatically, verifying its weaker ability to encapsulating oil. The results suggested that CNF with smaller diameter was more favorable for the construction of oleogels with higher OBC. It possibly benefited from the increased number of hydroxyl functionality on CNF surface and the enhanced hydrogen bonding interactions between CNF molecules and between CNF molecules with walnut oil molecules during oleogelation. The enhanced intermolecular noncovalent interactions not only favored the construction of a more compact and dense polysaccharide network for trapping liquid oil, but also elevated the ability of CNF factor to incorporating more oil molecules into the oleogel structure.

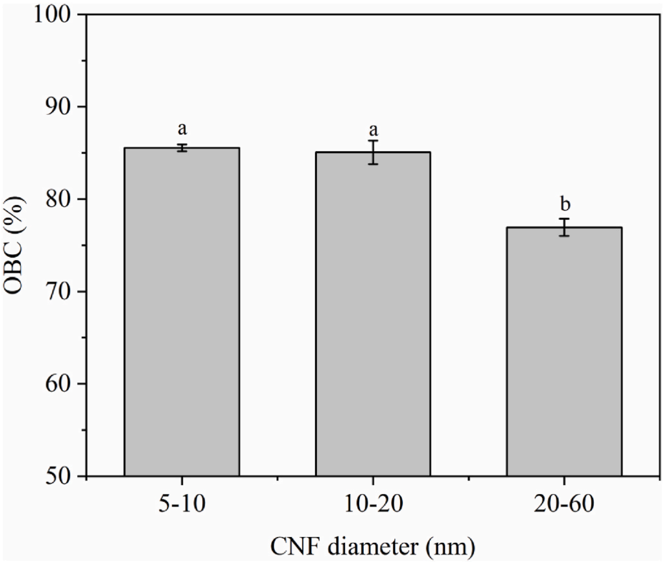

Fig. 4. The oil-binding capacity of oleogels with various CNF diameters.

The oil loss of oleogels at high temperature can reflect their thermal stability (Phoon & Henry, 2020). The appearances of oleogels after incubation at various temperatures were shown in Fig. S1A. No oil leakage was observed at 30 °C among all samples. With the temperature increased, the oil leakage became more obvious, especially in oleogels with CNF diameter of 20–60 nm, indicating the structure of the studied oleogels became looser. In consistent with Fig. S1A, oleogels with CNF diameters of 5–10 and 10–20 nm showed comparatively limited oil loss of 12.7% and 13.7% at 30 °C, respectively, while oleogel with CNF diameter of 20–60 nm showed elevated oil loss of 25.2% (Fig. S1B). With the increase of incubation temperature, the oil loss values gradually increased, while the oil loss of oleogel with CNF diameter of 10–20 nm increased faster. The oil loss values of the oleogel with CNF diameter of 20–60 nm (the highest value of 29.8% after heating at 90 °C) were largest than those with CNF diameters of 5–10 and 10–20 nm under the same studied temperatures (Fig. S1B). These results indicated that oleogels with small CNF diameter exhibited better thermal stability to resisting the destruction of oleogel network at high temperature. Again, this reflected the important role of hydrogen bonding on CNF surface in the stabilization of oleogel structure and the ability of this structure to holding liquid oil.

3.5. FTIR spectra and XRD pattern

The interactions between different CNFs and between CNF with walnut oil were characterized using Fourier transform-infrared spectroscopy (FTIR). From the FTIR spectra of different CNF powders (Fig. 5A), the broad peak at around 3455-3373 cm^{-1} was attributed to the stretching vibration of hydroxyl group in CNF. The minor peak at 2901-2904 cm^{-1} was due to C–H stretching vibration of cellulose

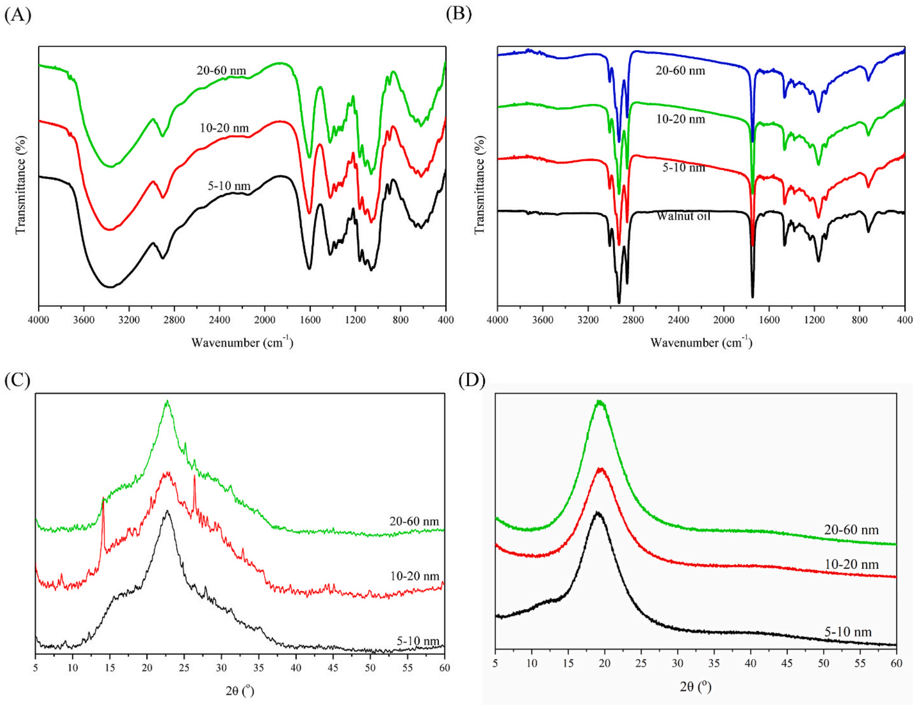

Fig. 5. FTIR spectra of CNFs (A) and oleogels (B) with various CNF diameters, respectively. X-ray diffraction patterns of CNFs (C) and oleogels (D) with various CNF diameters.

aliphatic function. The sharp peak at 1605-1608 cm^{-1} was mainly corresponded to C═O stretching vibration of -COONa (Li et al., 2023). Peaks around 1420-1316 cm^{-1} originated from the in-plane bending of C–H and C–O linkages, while peaks around 1162-1058 cm^{-1} were resulted from the signal overlap of C–O stretching vibration and O–H association. The small peak at 618 cm^{-1} was probably the signal of anomeric carbon (C1) of glucose unit. In Fig. 5A, relative to the peak at about 1060 cm^{-1}, the intensity of the carboxyl sodium signal at around 1606 cm^{-1} and the hydroxyl signal at around 3374 cm^{-1} were enhanced with the decrease of CNF diameter, while it was more obvious for the hydroxyl signal. It might indicate that with the deepening of cellulose fibrillation level and the reduction in CNF diameter, more glycosylated bonds (C–O–C) were hydrolyzed to hydroxyl groups (C–OH), and more hydroxyl groups in cellulose interior were exposed.

From the FTIR spectra of the homologous CNF-based oleogels (Fig. 5 B), all absorption peaks in the oleogel spectra were similar to the spectrum of the raw oil, indicating that walnut oil was the dominated component in oleogels, while no chemical reaction occurred during the interactions between walnut oil and CNFs (Li et al., 2023). Three sharp peaks appeared in the gel at 3009.9, 2926.9 and 2855.1 cm^{-1}. Comparing with walnut oil and CNF, it could be found that the peak at 3009.9 cm^{-1} mainly originated from the C–H stretching of walnut oil, and the peaks at 2926.9 and 2855.1 cm^{-1} were due to the CH_2 and CH_3 stretching vibration of walnut oil and CNF. The peak at 1746 cm^{-1} corresponded to the stretching of the C═O bond in walnut oil. The two peaks at 1465.2 and 1377.9 cm^{-1} corresponded to the C–H bending of the CH_3 and CH_2 groups associated with walnut oil and CNF. The peaks at 1164.3 and 1099.7 cm^{-1} represented the C–O stretching of C–O–H and C–O–C linkages, respectively. The small peak near 722 cm^{-1} was attributed to walnut oil and corresponded to the CH_2 stretching vibration. The FTIR spectra of the three CNF-based oleogels were not significantly different.

The XRD pattern provides information on the crystallinity and internal structure of the CNF powders and oleogel samples (Fig. 5C and D). For CNF, a characteristic reflection at $2\theta = 22.56°$ and its shoulder at $2\theta = 16.10°$ were observed, indicating the 002 and 10-1 planes of cellulose crystal, respectively (Fig. 5C). There was no significant difference in the XRD diffractograms of the three oleogels, and only one broad peak appeared around $2\theta = 19.3°$ (Fig. 5D andTable 3), which might be attributed to the co-crystallization of CNF and some oil molecules that was adjacent to CNF molecules during freeze-drying (Meng, Qi, Guo, Wang, & Liu, 2018). The crystal size decreased slightly with the increase of CNF diameter. A short crystal plane spacing of about 4.60 Å was calculated, which indicated that new crystals were generated during the freeze-drying process.

3.6. Rheological measurement

3.6.1. Strain sweep

The rheological properties of oleogels with different CNF diameters were evaluated to compare their deformation and viscoelastic properties. Fig. 6 shows the linear viscoelastic region (LVR) and yield strain results obtained using strain sweep measurements. From Fig. 6A, at lower strain, the storage modulus (*G*') of all three types of oleogels was always larger than the loss modulus (*G*"), indicating the solid-like behavior of the CNF-based oleogels. The parameters considered for LVR characterization are the limiting shear strain γ_{max} and the corresponding dynamic yield stress σ_{max}. All oleogel samples exhibited comparable LVR range (γ_{max} of 0.115%, 0.137% and 0.110%) (Fig. 6B), in which *G*′ and *G*″ were frequently constant. The *G*' values of CNF-based samples within LVR followed the order of 5–10 nm (117.05 kPa) > 10–20 nm (95.09 kPa) > 20–60 nm (80.45 kPa), which demonstrated that the oleogel strength decreased with the CNF diameter increased. The oleogel constructed with CNF diameter of 5–10 nm had the strongest gel strength (*G*'), indicating a higher structuring level of liquid oil,

Table 3
XRD parameters of oleogels with different CNF diameters.

CNF diameter (nm)	2*θ* (°)	Crystalline dimension *D* (nm)	Short spacing *d* (Å)
5–10	19.19	1.43	4.62
10–20	19.37	1.37	4.58
20–60	19.15	1.31	4.63

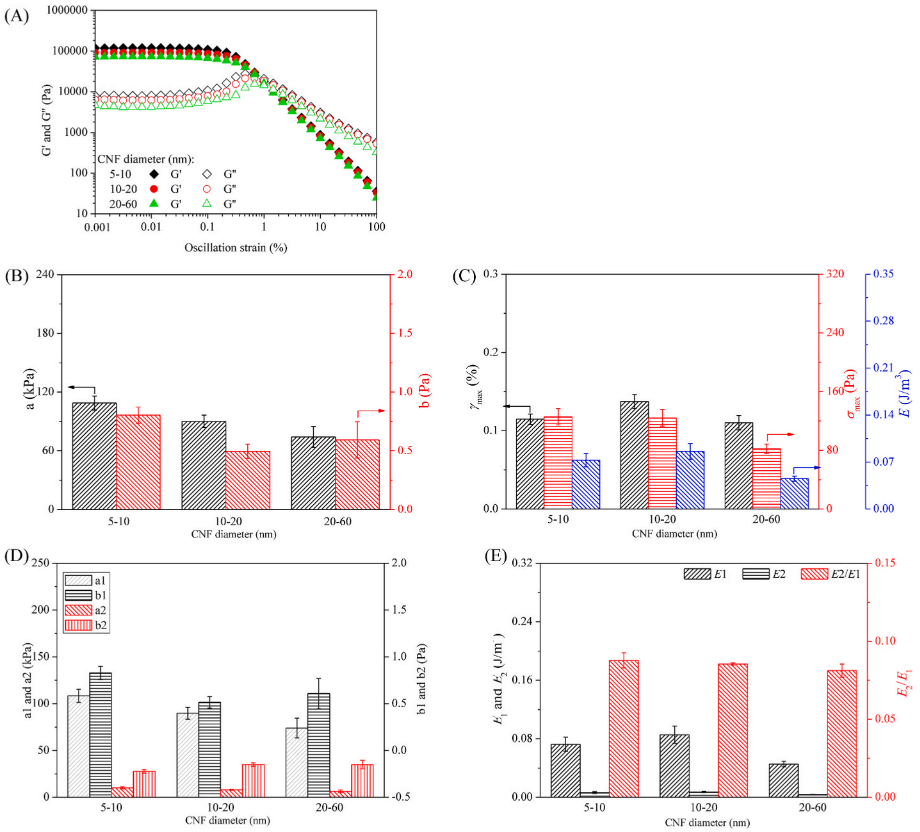

Fig. 6. Strain sweep of oleogels with various CNF diameters. (A) G' and G'' curves of oleogels, (B) fitting analysis results of shear stress *vs.* shear strain in LVR, (C) limiting shear strain (γ_{max}), limiting shear stress (σ_{max}) and stabilization energy (E) in LVR of oleogels, (D) fitting analysis results of elastic stress ($\sigma_{elastic}$) and viscous stress ($\sigma_{viscous}$) *vs.* shear strain, (E) stabilization energy contributed by $\sigma_{elastic}$ and $\sigma_{viscous}$.

and could be attributed to the enhanced hydrogen bonding interactions for oleogelation. After the strain exceeded the LVR range, the functional correlation between the stress and the strain no longer followed the linear characteristic. As a result, G' decreased rapidly (large deformations) with increasing strain, while G'' first increased and then rapidly decreased. A cross point (structural yield) of G' and G'' curves was observed at higher strain level (Naeli, Milani, Farmani, & Zargaraan, 2020), which implied the complete destruction of the colloidal structure and the appearance of flow characteristics for the system. From Fig. 6A, the yield of oleogels with CNF diameters of 5–10 nm and 10–20 nm appeared at comparable strain level (0.97%), which was some earlier than that (1.14%) with CNF diameter of 20–60 nm.

The linear fitting results of σ vs γ in LVR verified the difference in gel strength (Fig. 6C). In Eq. (5), the slope "a (Pa)" quantifies the overall resistance to the deformation of oleogel network in LVR interval, and hence provides another measurement of gel strength (Borderías et al., 2020). The independent coefficient "*b*" (Pa) is the initial stress. In general, the slope "a" was reduced in the oleogel (108.8, 90.1 and 74.3 kPa, $p < 0.05$, Fig. 6C) with the CNF diameter range increased from 5-10 nm to 20–60 nm, which followed the same order as the G', and indicated that CNF diameter negatively affected the gel strength.

The "E" magnitude (J/m^3) represents the total energy (per volume unit) in the linear deformation of the gel network in the LVR range, which quantifies the energy stability of the gel network in the LVR. In Fig. 6C, highest "E" value was conferred on CNF-based oleogel with CNF diameter of 10–20 nm, which meant the best energy stability to maintain the compact gel structure. This fact corroborated the structural benefit conferred by CNF with diameter of 10–20 nm for the energy stability of the oleogel network. Oppositely, the worst energy stability was detected for oleogel with CNF diameter of 20–60 nm.

In Fig. 6D and E, the stress value in LVR was decomposed into elastic ($\sigma_{elastic}$) and viscous components ($\sigma_{viscous}$) following our previous report (Li et al., 2024), which was used to compare the contribution of elastic and viscous factors on the oleogel structure. From Fig. 6E, the E_2/E_1 ratio of oleogels with CNF diameters of 5–10 and 10–20 nm was slightly higher than the ratio of oleogel with CNF diameter of 20–60 nm, indicating a higher contribution of viscous components on the construction and stabilization of oleogel network with reduced CNF diameters.

3.6.2. Frequency sweep and viscosity sweep

The result of frequency sweep provides the mechanical spectra analysis of the CNF-based oleogels. As shown in Fig. 7A, the G' values of all oleogels were greater than the G″ values over the frequency range of 0.01–100 Hz, which identified the solid-like behavior. The frequency-dependent behavior of complex modulus (G^* values) within the frequency range of 0.1–10 s^{-1} was examined by Fig. 7B, in which the parameters of power-law model (G_0* and n*) were calculated. Here, G_0* presents the G^* modulus at angular frequency of 1 rad/s (equivalent to regular frequency of 0.1592 Hz). In Fig. 7B, G_0* decreased with the increase of CNF diameter, which was in consistence with the strain sweep results in Section 3.6.1. The n* exponent is employed to ascertain the elastic behavior of CNF-based oleogels. As seen from Fig. 7B, the n* values of the oleogel samples were in the range of 0.0332–0.0361, which confirmed the elastic behavior of the samples (Naeli, Milani, Farmani, & Zargaraan, 2022). In consistent with Fig. 6E, slightly more elastic constitute (lower n*) in the oleogel structure was observed for the oleogel with CNF diameter of 20–60 nm. At higher frequency of >10 Hz, both G' and G'' parameters were slightly shifted to higher values with an increase in the frequency, indicating an increased dependent manner.

Dynamic viscosity sweep tests can provide valuable information about the mechanical processing-induced viscoelastic changes of oleogels (Fig. 7C). The viscosity decreased with the increase of shear rate

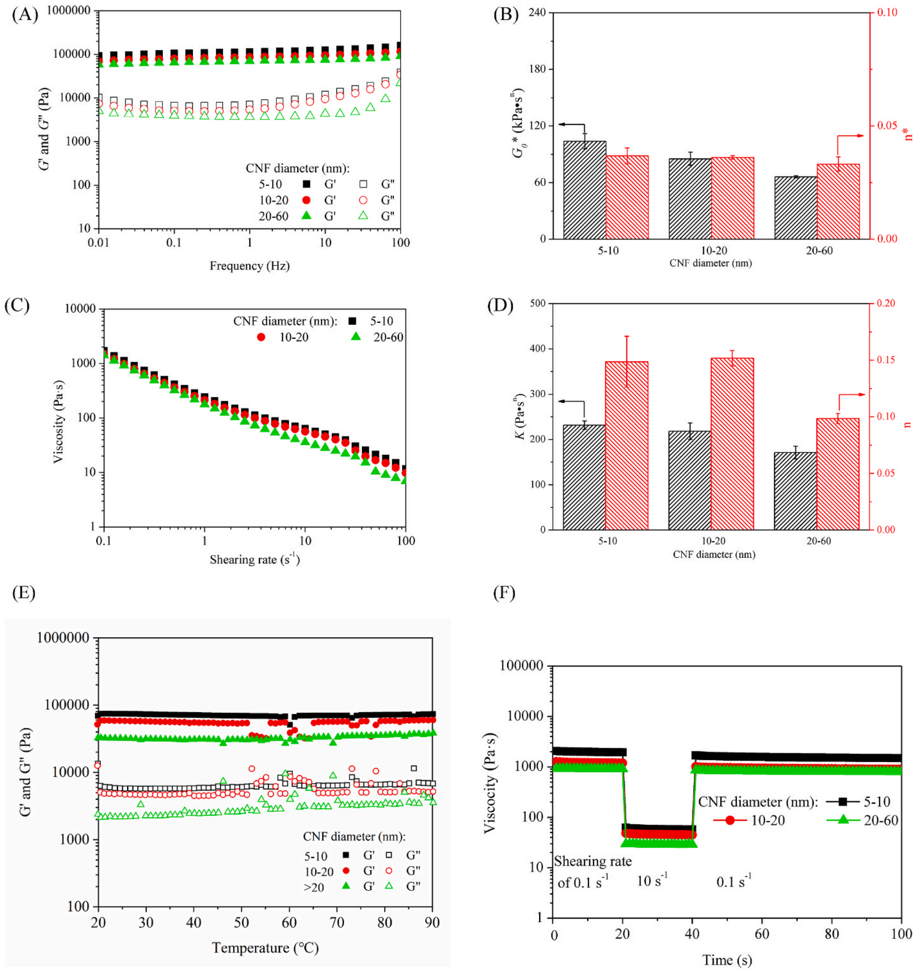

Fig. 7. Frequency sweep, flow measurement, temperature sweep and thixotropy test of oleogels with various CNF diameters. (A) Frequency sweep curves of oleogels, (B) fitting analysis results of frequency dependent of G^* in 0.01–10 Hz. (C) viscosity curves. (D) fitting analysis results of $\log_2\eta$ *vs.* $\log_2$ within of ≤ 1 s^{-1}. (E) temperature sweep curves. (F) thixotropy test curves.

from 0.1 to 100 s^{-1}, indicating that all studied oleogels exhibited shear thinning behavior. The initial values of apparent viscosity at low shear rate of 0.1 s^{-1} followed the order of 5–10, 10–20 and 20–60 nm. The empirical constant (*K* index) was decreased with the larger CNF diameters, which was in consistent with the results of Figs. 6E and 7B. The flow behavior index (n) from the linear fitting of the flow curves with shear rate ranging from 0.1 to 1.0 s^{-1} was calculated (Fig. 7C, Li et al., 2024). For all oleogels, the n values were smaller than 1 (Fig. 7D), confirming the shear thinning behavior. Larger deviations of the power-law exponent (n) value from 1 imply that the sample is more susceptible to shear-thinning (Zhu, Meng, Li, Jiang, & Liu, 2013). Thus, oleogel with CNF diameter of 10–20 nm had the strongest tendency to resisting shear thinning, which was agree with the γ_{max} results in Fig. 6C.

3.6.3. *Temperature sweep and thixotropic tests*

To study the heat-induced changes occurring in the viscoelastic properties of the oleogels, temperature sweep was performed by determining G' and G'' moduli as a function of temperature from 20 to 90 °C (Fig. 7E). As seen in Fig. 7E, the G' was higher than G'' in all tested oleogels, indicating less changes in the viscoelastic nature of the samples in the swept temperature range. In addition, the G' moduli of all oleogels were consistent with an increase in temperature, indicating their thermal stability. Similar behaviors were observed in cellulose-rich sunflower oil oleogels (Jiang et al., 2018) and our previous study (Li et al., 2023).

Thixotropy is an important rheological property for evaluating the potential applications of oleogels in food manufacturing. To further understand the time-dependent rheological and structural-recovery properties of these viscoelastic substances, 3ITT tests were performed at alternating shear rates (0.1, 10 and 0.1 s^{-1}). Initially, the apparent viscosity of the oleogels slightly decreased with shear time remaining (Fig. 7F). When the shear rate was changed to 10 s^{-1}, the viscosity immediately decreased, which indicated a shear thinning behavior (Fig. 7F). Sufficient rotation stress could destroy the connection between oleogel network structures and reduce the flow resistance (Jiang et al., 2018). Subsequently, when the stable shear rate was set back to 0.1 s^{-1}, the viscosity was instantly recovered owing to the reversible elastic gel network, which eliminated the damage caused by the external mechanical force on the oleogels. All the oleogel samples showed good thixotropic recovery with the viscosity recovered above 75% (Fig. 7F).

3.7. *Texture analysis*

The time curve of the oleogel during puncture was shown in Fig. 8. The curve showed an upward trend during the puncture to the specified position, without rupture peak or sudden drop in the force value, indicating that the oleogel was not damaged and had a stable structure. There was no significant difference in the hardness of oleogels with CNF diameters of 5–10 nm and 10–20 nm, which was 0.46 N. When the CNF diameter increased, the hardness (0.26 N) and AUC (1.07 N s) of the oleogels with CNF diameter of 20–60 nm decreased significantly, indicating that the resistance encountered during the puncture was smaller,

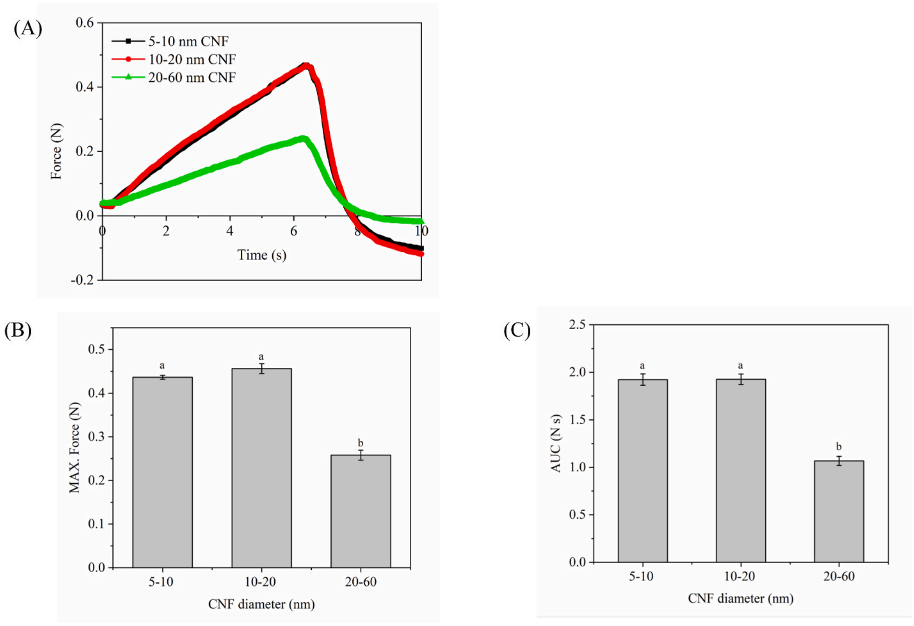

Fig. 8. Force-time curves (A), maximum force (B) and area under the curve (C) of oleogels with different CNF diameters. a–d: different letters indicate significant differences ($p < 0.05$).

and the oleogel was more loosely structured. This result verified again the importance of the intermolecular hydrogen bond of CNF in the construction of oleogel with comparable mechanical strength.

4. Conclusions

Oleogels with different CNF diameters (5–10 nm, 10–20 nm and 20–60 nm) were prepared by the emulsion-templated method, and their structural and physical properties were tested. The CNF diameter showed significantly influence on the structure, rheological and textural properties of the oleogels. In emulsion stage, smaller CNF diameter (5–10 and 10–20 nm) resulted in emulsions with smaller droplet size and higher interfacial activity, which directed to a much more stable emulsion structure. In oleogel stage, oleogels with CNF diameters of 5–10 and 10–20 nm showed more compact microstructure, enhanced OBC and less oil loss after high temperature processing, and higher gelation strength compared to oleogel with CNF diameter of 20–60 nm. It clearly demonstrated that smaller CNF diameter could provide more hydroxyl sits for enhanced hydrogen bonding interactions between CNF molecules and between CNF molecules with walnut oil molecules during oleogelation. It benefited the fabrication of a more compact and stable oleogel structure that could firmly hold more vegetable oil molecules.

Declaration of generative AI in scientific writing

The authors declare that they never used generative AI and AI-assisted technologies in the writing process.

CRediT authorship contribution statement

Yuxuan Zou: Writing – original draft, Investigation. **Yang Tian:** Writing – original draft, Methodology, Formal analysis. **Bing Zhao:** Data curation. **Jienan Li:** Resources. **Jia Luo:** Writing – review & editing, Validation. **Jun Sheng:** Writing – review & editing. **Xiufen Li:** Writing – review & editing, Project administration, Funding acquisition.

Declaration of competing interest

The authors declare that they have no known competing financial interests or personal relationships that could have appeared to influence the work reported in this paper.

Data availability

Data will be made available on request.

Acknowledgement

This work was supported by National Natural Science Foundation of China (32160564), Yunnan Fundamental Research Projects (202401AT070241), Yunnan Innovation Team of Food and Drug Homologous Functional Food (202305AS350025), Yunnan Province-City Integration Project (202302 AN360002), and Yunnan Province ten thousand planned industrial technology leading talents project (YNWR-CYJS-2020-010). The authors also want to thank Runzhe Liu (senior engineering) from Yunnan Phosphate Chemical Group Co. Ltd (Kunming, Yunnan, China) for his warmly assistance in the determination of the surface tension of CNF solutions.

Appendix A. Supplementary data

Supplementary data to this article can be found online at https://doi.org/10.1016/j.foodhyd.2024.110149.

References

Arcari, M., Geue, T., Mezzenga, R., Nyström, G., & Fischer, P. (2019). Designing cellulose nanofibrils for stabilization of fluid interfaces. *Biomacromolecules, 20*(12), 4574–4580. https://doi.org/10.1021/acs.biomac.9b01384

Bascuas, S., Hernando, I., Moraga, G., & Quiles, A. (2019). Structure and stability of edible oleogels prepared with different unsaturated oils and hydrocolloids. *International Journal of Food Science and Technology, 55*, 1458–1467. https://doi.org/10.1111/ijfs.14469

Bergfreund, J., Sun, Q. Y., Fischer, P., & Bertsch, P. (2019). Adsorption of charged anisotropic nanoparticles at oil-water interfaces. *Nanoscale Advances, 11*, 4308–4312. https://doi.org/10.1039/C9NA00506D

Borderías, A. J., Tovar, C. A., Domínguez-Timón, F., Díaz, M. T., Pedrosa, M. M., & Moreno, H. M. (2020). Characterization of healthier mixed surimi gels obtained through partial substitution of myofibrillar proteins by pea protein isolates. *Food Hydrocolloids, 107*, Article 105976. https://doi.org/10.1016/j.foodhyd.2020.105976

Cano-Sarmiento, C., Téllez-Medina, D. I., Viveros-Contreras, R., Cornejo-Mazón, M., Figueroa-Hernández, C. Y., García-Armenta, E., et al. (2018). Zeta potential of food matrices. *Food Engineering Reviews, 10*, 113–138. https://doi.org/10.1007/s12393-018-9176-z

Carrillo, C. A., Nypelö, T. E., & Rojas, O. J. (2015). Cellulose nanofibrils for one-step stabilization of multiple emulsions (W/O/W) based on soybean oil. *Journal of Colloid and Interface Science, 445*, 166–173. https://doi.org/10.1016/j.jcis.2014.12.028

Cong, Y. X., Zhang, W. N., Liu, C. S., & Huang, F. H. (2020). Composition and oil-water interfacial tension studies in different vegetable oils. *Food Biophysics, 15*, 229–239. https://doi.org/10.1007/s11483-019-09617-8

Dickinson, E. (2019). Strategies to control and inhibit the flocculation of protein-stabilized oil-in-water emulsions. *Food Hydrocolloids, 96*, 209–223. https://doi.org/10.1016/j.foodhyd.2019.05.021

Du, H., Liu, W., Zhang, M., Si, C., Zhang, X., & Li, B. (2019). Cellulose nanocrystals and cellulose nanofibrils based hydrogels for biomedical applications. *Carbohydrate Polymers, 209*, 130–144. https://doi.org/10.1016/j.carbpol.2019.01.020

Goi, Y., Fujisawa, S., Saito, T., Yamane, K., Kuroda, K., & Isogai, A. (2019). Dual functions of TEMPO-oxidized cellulose nanofibers in oil-in water emulsions: A pickering emulsifier and a unique dispersion stabilizer. *Langmuir, 35*, 10920–10926. https://doi.org/10.1021/acs.langmuir.9b01977

Habibi, Y., Lucia, L. A., & Rojas, O. J. (2010). Cellulose nanocrystals: Chemistry, self-assembly, and applications. *Chemical Reviews, 110*(6), 3479–3500. https://doi.org/10.1021/cr900339w

Hu, X., Jiang, Q., Du, L., & Meng, Z. (2023). Edible polysaccharide-based oleogels and novel emulsion gels as fat analogues: A review. *Carbohydrate Polymers, 322*(15), Article 121328. https://doi.org/10.1016/j.carbpol.2023.121328

Jiang, Y., Liu, L., Wang, B., Sui, X., Zhong, Y., Zhang, L. P., et al. (2018). Cellulose-rich oleogels prepared with an emulsion-templated approach. *Food Hydrocolloids, 77*, 460–464. https://doi.org/10.1016/j.foodhyd.2017.10.023

Lee, J., Wi, G., & Choi, M.-J. (2023). The rheological properties and stability of gelled emulsions applying to κ-carrageenan and methyl cellulose as an animal fat replacement. *Food Hydrocolloids, 136*, Article 108243. https://doi.org/10.1016/j.foodhyd.2022.108243

Li, X., Guo, G., Zou, Y., Luo, J., Sheng, J., Tian, Y., et al. (2023). Development and characterization of walnut oleogels structured by cellulose nanofber. *Food Hydrocolloids, 142*, Article 108849. https://doi.org/10.1016/j.foodhyd.2023.108849

Li, X., Zou, Y., Zhao, B., Luo, J., Li, J., Sheng, J., et al. (2024). Effects of drying method and oil type on edible polyunsaturated oleogels co-structured by hydroxylpropyl methyl cellulose and xanthan gum. *International Journal of Biological Macromolecules, 256*, Article 128551. https://doi.org/10.1016/j.ijbiomac.2023.128551

Lu, Y., Li, J., Ge, L., Xie, W., & Wu, D. (2021). Pickering emulsion stabilized with fbrous nanocelluloses: Insight into fiber fexibility-emulsifying capacity relations. *Carbohydrate Polymers, 255*, Article 117483. https://doi.org/10.1016/j.carbpol.2020.117483

Lv, S., Zhou, H., Bai, L., Rojas, O. J., & McClements, D. J. (2021). Development of food-grade Pickering emulsions stabilized by a mixture of cellulose nanofibrils and nanochitin. *Food Hydrocolloids, 113*, Article 106451. https://doi.org/10.1016/j.foodhyd.2020.106451

Meng, Z., Qi, K., Guo, Y., Wang, Y., & Liu, Y. (2018). Physical properties, microstructure, intermolecular forces, and oxidation stability of soybean oil oleogels structured by different cellulose ethers. *European Journal of Lipid Science and Technology, 120*(6), Article 1700287. https://doi.org/10.1002/ejlt.201700287

Naeli, M. H., Milani, J. M., Farmani, J., & Zargaraan, A. (2020). Development of innovative ethyl cellulose-hydroxypropyl methylcellulose biopolymer oleogels as low saturation fat replacers: Physical, rheological and microstructural characteristics. *International Journal of Biological Macromolecules, 156*(2020), 792–804. https://doi.org/10.1016/j.ijbiomac.2020.04.087

Naeli, M. H., Milani, J. M., Farmani, J., & Zargaraan, A. (2022). Developing and optimizing low-saturated oleogel shortening based on ethyl cellulose and hydroxypropyl methyl cellulose biopolymers. *Food Chemistry, 369*, Article 130963. https://doi.org/10.1016/j.foodchem.2021.130963

Ni, Y., Fan, L., & Sun, Y. (2020). Interfacial properties of cellulose nanoparticles with different lengths from ginkgo seed shells. *Food Hydrocolloids, 109*, Article 106121. https://doi.org/10.1016/j.foodhyd.2020.106121

Patel, A. R., Cludts, N., Sintang, M. D. B., Lewille, B., Lesaffer, A., & Dewettinck, K. (2014). Polysaccharide-based oleogels prepared with an emulsion-templated approach. *ChemPhysChem, 15*, 3435–3439. https://doi.org/10.1002/cphc.201402473

Perumal, A. B., Nambiar, R. B., Moses, J. A., & Anandharamakrishnan, C. (2022). Nanocellulose: Recent trends and applications in the food industry. *Food Hydrocolloids, 127*, Article 107484. https://doi.org/10.1016/j.foodhyd.2022.107484

Phoon, P. Y., & Henry, C. J. (2020). Fibre-based oleogels: Effect of the structure of insoluble fibre on its physical properties. *Food & Function, 11*, 1349–1361. https://doi.org/10.1039/C9FO02431J

Piao, X., Li, J., Zhao, Y., Guo, L., Zheng, B., Zhou, R., et al. (2022). Oxidized cellulose nanofibrils-based surimi gel enhancing additives: Interactions, performance and mechanisms. *Food Hydrocolloids, 133*, Article 107893. https://doi.org/10.1016/j.foodhyd.2022.107893

Velásquez-Cock, J., Serpa, A., Vélez, L., Gañán, P., Hoyos, G. C., Castro, C., et al. (2019). Influence of cellulose nanofibrils on the structural elements of ice cream. *Food Hydrocolloids, 87*, 204–213. https://doi.org/10.1016/j.foodhyd.2018.07.035

Wang, Q., Espert, M., Larrea, V., Quiles, A., Salvador, A., & Sanz, T. (2023). Comparison of different indirect approaches to design edible oleogels based on cellulose ethers. *Food Hydrocolloids, 134*, Article 108007. https://doi.org/10.1016/j.foodhyd.2022.108007

Yu, S., Peng, G., & Wu, D. (2024). Effect of surface acetylation of chitin nanocrystals on the preparation and viscoelasticity of sunflower seed oil-in-water Pickering emulsions. *International Journal of Biological Macromolecules, 254*, Article 127883. https://doi.org/10.1016/j.ijbiomac.2023.127883

Zhao, W., Wei, Z., & Xue, C. (2021). Recent advances on food-grade oleogels: Fabrication, application and research trends. *Critical Reviews in Food Science and Nutrition*, 7659–7676. https://doi.org/10.1080/10408398.2021.1922354

Zhu, J., Liu, L., Li, X., Zhang, Q., Wang, Z., Chen, N., et al. (2024). Construction of soybean oil bodies-xanthan gum composite oleogels by emulsion-templated method: Preparation, characterization, and stability analysis. *Food Hydrocolloids, 149*, Article 109526. https://doi.org/10.1016/j.foodhyd.2023.109526

Zhu, X., Meng, Z., Li, J., Jiang, J., & Liu, Y. (2013). Effect of gelators on physical properties, crystal morphologies of organogel oils. *Journal of the Chinese Cereals and Oils Association, 28*(10), 37–43 (in Chinese).